

## Coupling of electrical and mechanical switching in nanoscale ferroelectrics

Ye Cao, Qian Li, Long-Qing Chen, and Sergei V. Kalinin

Citation: [Applied Physics Letters](#) **107**, 202905 (2015); doi: 10.1063/1.4935977

View online: <http://dx.doi.org/10.1063/1.4935977>

View Table of Contents: <http://scitation.aip.org/content/aip/journal/apl/107/20?ver=pdfcov>

Published by the [AIP Publishing](#)

---

### Articles you may be interested in

[Nanoscale mechanical switching of ferroelectric polarization via flexoelectricity](#)

Appl. Phys. Lett. **106**, 022904 (2015); 10.1063/1.4905837

[Wake-up effects in Si-doped hafnium oxide ferroelectric thin films](#)

Appl. Phys. Lett. **103**, 192904 (2013); 10.1063/1.4829064

[Scaling of structure and electrical properties in ultrathin epitaxial ferroelectric heterostructures](#)

J. Appl. Phys. **100**, 051609 (2006); 10.1063/1.2337363

[Mechanical stress effect on imprint behavior of integrated ferroelectric capacitors](#)

Appl. Phys. Lett. **83**, 728 (2003); 10.1063/1.1593830

[In situ observation of ferroelectric 90°-domain switching in epitaxial Pb\(Zr,Ti\)O<sub>3</sub> thin films by synchrotron x-ray diffraction](#)

Appl. Phys. Lett. **79**, 2444 (2001); 10.1063/1.1406981

---

A promotional banner for Applied Physics Reviews. On the left is a thumbnail of a review article cover titled 'AIP Applied Physics Reviews' with a diagram of a layered structure. The main text reads 'NEW Special Topic Sections' in large white letters on a blue background. Below this, it says 'NOW ONLINE' in yellow, followed by 'Lithium Niobate Properties and Applications: Reviews of Emerging Trends' in white. The AIP Applied Physics Reviews logo is in the bottom right corner.

**NEW Special Topic Sections**

**NOW ONLINE**  
Lithium Niobate Properties and Applications:  
Reviews of Emerging Trends

**AIP** Applied Physics  
Reviews

## Coupling of electrical and mechanical switching in nanoscale ferroelectrics

Ye Cao,<sup>1,2</sup> Qian Li,<sup>1,2</sup> Long-Qing Chen,<sup>3</sup> and Sergei V. Kalinin<sup>1,2</sup>

<sup>1</sup>Center for Nanophase Materials Sciences, Oak Ridge National Laboratory, Oak Ridge, Tennessee 37831, USA

<sup>2</sup>Institute for Functional Imaging of Materials, Oak Ridge National Laboratory, Oak Ridge, Tennessee 37831, USA

<sup>3</sup>Department of Materials Science and Engineering, The Pennsylvania State University, University Park, Pennsylvania 16802, USA

(Received 25 August 2015; accepted 31 October 2015; published online 19 November 2015)

While electric field induced ferroelectric switching has been extensively studied and broadly utilized, pure mechanical switching via flexoelectric effect has recently opened up an alternative method for domain writing due to their highly localized, electrically erasable and electric damage free characteristics. Thus far, few studies have been made on the coupling effect of electro-mechanical switching in ferroelectric materials, likely due to the experimental difficulty in the accurate definition of the tip-surface contact area and in the identification of mechanical contribution from electrical effect. Here, we employed self-consistent phase-field modeling to investigate the bi-polar switching behavior of (001) oriented  $\text{Pb}(\text{Zr}_{0.2}\text{Ti}_{0.8})\text{O}_3$  thin film under concurrent electric and strain field created via a piezoresponse force microscope probe. By separating the effects from electric field, homogeneous strain and strain gradient, we revealed that the homogeneous strain suppresses the spontaneous polarization and accordingly increases the coercive field, and the strain gradient favors unipolar switching and inhibit it in the reverse direction, thus causing lateral offset of the hysteresis loop. The uncertainty of flexoelectric coefficients and the influence of flexocoupling coefficients on switching have also been discussed. Our study could necessitate further understanding of the electric, piezoelectric, and flexoelectric contribution to the switching behavior in nanoscale ferroelectric oxides. © 2015 AIP Publishing LLC. [<http://dx.doi.org/10.1063/1.4935977>]

The strong coupling between electric polarization and mechanical strain endows ferroelectric materials' unique electromechanical properties, including piezoelectric and flexoelectric effects. While piezoelectricity describes the linear dependence of electric polarization ( $P_i$ ) on the homogeneous strain ( $\varepsilon_{jk}$ ), flexoelectricity relates the polarization with the inhomogeneous strain, or the strain gradient ( $\partial\varepsilon_{kl}/\partial x_j$ ). In the absence of an applied electric field, the combined piezoelectric and flexoelectric contributions to the polarization is represented by

$$P_i = d_{ijk}\varepsilon_{jk} + \mu_{ijkl}\frac{\partial\varepsilon_{kl}}{\partial x_j} \quad (i, j, k, l = 1 \sim 3), \quad (1)$$

where  $d_{ijk}$  and  $\mu_{ijkl}$  are the piezoelectric and flexoelectric polarization tensors, respectively. Piezoelectric phenomena in ferroelectric materials have been extensively studied and led to broad applications in various electronic devices such as sensors and actuators.<sup>1-3</sup> By comparison, flexoelectricity is much less explored thus far. This is due to the relatively small magnitude of flexoelectric coefficients (FEC) ( $\mu_{ijkl}$  on the order of nC/m),<sup>4,5</sup> making it negligible compared to the piezoelectric effect in bulk ferroelectrics. However, in nanoscale material systems, the strain gradient could be enhanced to  $10^8\text{ m}^{-1}$ , and consequently, the flexoelectric effect becomes significant. Since then, there have been extensive studies<sup>5,6</sup> on the symmetry<sup>7-9</sup> and magnitude<sup>10-12</sup> of flexoelectric coefficient, the effect of flexoelectricity on domain walls,<sup>13-16</sup> domain pattern,<sup>17,18</sup> and polarization rotations,<sup>19</sup> and the flexoelectricity-driven domain switching.<sup>20-23</sup> Gruverman *et al.* introduced large strain gradient in  $\text{Pb}(\text{Zr}_{0.2}\text{Ti}_{0.8})\text{O}_3$  (PZT) thin films by bending the substrates and thereby switched the polarization.<sup>24</sup> Strong

flexoelectric effect can also be associated with ferroelectric domain walls where the strain remarkably changes across nanometric wall thickness, which has been used to explain the fact that Ising-like  $180^\circ$  domain walls are mixed with Neel and Bloch polarization components in tetragonal  $\text{BaTiO}_3$ .<sup>13,16</sup> Recently, the mechanical tip-induced ferroelectric switching was observed in ultra-thin  $\text{BaTiO}_3$  thin film and was ascribed to the flexoelectric effect, thus providing possibilities of effective mechanical-driven domain writing in the absence of conventional electric field.<sup>20,22,25</sup> In spite of these studies, nanoscale ferroelectric switching driven by coupled electrical and mechanical fields, as is the scenario in piezoresponse force microscopy/spectroscopy (PFM/S),<sup>26-30</sup> appear to be less satisfactorily addressed. This can be due to experimental difficulties, such as the fact that the dead layers that are usually formed on top of a ferroelectric surface could be readily damaged by large tip loading forces, and the tip-sample contact areas are ever-changing under different pressure loads; both effects make it difficult to compare the piezoresponses when the switching hysteresis loops are measured. The extremely thin films are unsustainable to large electric fields and could result in dielectric breakdown. Thus, the film thickness and the magnitude of pressure load may be critical to ensure both an observable flexoelectric effect and a sustainable film. Even so, it is experimentally difficult to distinguish and weigh the contributions of mechanical load and electric field. To unravel the mechanical/electrical coupling effect to ferroelectric switching and overcome the experimental limitations, a physics-based theoretical approach is imperative.

In this work, we employed phase-field modeling<sup>31</sup> to analyze the bipolar ferroelectric switching properties of a local tip-ferroelectric nanojunction,<sup>32-35</sup> which approximates the

geometry found in PFM. We separately studied the effect of piezoelectricity and flexoelectricity on bias induced switching in  $\text{Pb}(\text{Zr}_{0.2}\text{Ti}_{0.8})\text{O}_3$  thin film with a range of tip pressure load. We found that the tip load suppresses the remnant polarization and symmetrically increases the coercive bias and critical voltage of ferroelectric domain breakdown. The strain gradient from the tip load induces a unidirectional flexoelectric field regardless of the external bias direction and offsets the hysteresis loop. Our work may provide some understanding on the electromechanical coupled ferroelectric switching processes in the PFM settings.

In the phase-field simulation, the temporal evolution of ferroelectric polarization vector is modeled by numerically solving the time-dependent Landau-Ginzburg-Devonshire (LGD) equations<sup>36</sup>

$$\frac{\partial P_i(\mathbf{x}, t)}{\partial t} = -L \frac{\delta F_{\text{total}}}{\delta P_i(\mathbf{x}, t)}, \quad i = 1, 2, 3, \quad (2)$$

in which  $P_i$  is the polarization vector,  $t$  is the time,  $L$  is the kinetic coefficient related to the domain movement, and  $F_{\text{total}}$  is the total free energy, which can be expressed as

$$F_{\text{total}} = \int_V [f_{\text{land}}(P_i) + f_{\text{elas}}(P_i, \varepsilon_{kl}) + f_{\text{elec}}(P_i, E_i) + f_{\text{grad}}(\nabla P_i) + f_{\text{flexo}}(P_i, \varepsilon_{kl}, \nabla P_i, \nabla \varepsilon_{kl})] dV, \quad (3)$$

in which  $\varepsilon_{kl}$  and  $E_i$  are strain and electric field components.  $f_{\text{land}}(P_i)$ ,  $f_{\text{grad}}(\nabla P_i)$ ,  $f_{\text{elas}}(P_i, \varepsilon_{ij})$ , and  $f_{\text{elec}}(P_i, E_i)$  represent the LGD free energy density, the gradient energy density, the elastic energy density, and the electrostatic energy density, respectively. Details of each of the energy density expressions are from literature.<sup>37</sup>  $f_{\text{flexo}}(P_i, \varepsilon_{kl}, \nabla P_i, \nabla \varepsilon_{kl})$  denotes the flexoelectric energy density written as<sup>38</sup>

$$\begin{aligned} f_{\text{flexo}}(P_i, \varepsilon_{kl}, \nabla P_i, \nabla \varepsilon_{kl}) &= \frac{1}{2} f_{ijkl} \left( \frac{\partial P_k}{\partial x_l} \varepsilon_{ij} - \frac{\partial \varepsilon_{ij}}{\partial x_l} P_k \right) \\ &= \frac{1}{2} F_{ijkl} \left( \frac{\partial P_k}{\partial x_l} \sigma_{ij} - \frac{\partial \sigma_{ij}}{\partial x_l} P_k \right), \end{aligned} \quad (4)$$

in which  $f_{ijkl}$  (unit: V) and  $F_{ijkl}$  (unit:  $\text{Vm}^2\text{N}^{-1}$ ) are the flexocoupling coefficient (FCC) tensors. The relations between  $f_{ijkl}$ ,  $F_{ijkl}$ , and  $\mu_{ijkl}$  are  $f_{ijkl} = c_{ijmn} F_{mnlk}$ ,  $\mu_{ijkl} = \varepsilon_0 \chi_{mn} f_{mnlk}$ , where  $c_{ijmn}$  is the elastic tensor,  $\varepsilon_0$  is the vacuum permittivity, and  $\chi_{mn}$  is the susceptibility. The driving force from the flexoelectric energy density is calculated through

$$\frac{\delta f_{\text{flexo}}}{\delta P_k} = \frac{\partial f_{\text{flexo}}}{\partial P_k} - \frac{\partial}{\partial x_l} \left( \frac{\partial f_{\text{flexo}}}{\partial P_k / \partial x_l} \right) = -F_{ijkl} \frac{\partial \sigma_{ij}}{\partial x_l} = -E_k^f, \quad (5)$$

where  $E_k^f$  is called the flexoelectric field. Since the electrostatic energy driving force is actually the electric field, i.e.,  $\delta f_{\text{elec}} / \delta P_k = -E_k$ , the flexoelectric driving force act as an additional electric field besides the applied one. For cubic symmetry, the flexoelectric tensor has three independent components  $F_{1111}$ ,  $F_{1122}$ , and  $F_{1221}$ .<sup>7-9</sup> By using the Voigt notation  $F_{11} = F_{1111}$ ,  $F_{12} = F_{1122}$ , and  $F_{44} = 2F_{1221}$ , Eq. (5) can be expanded as

$$E_1^f = F_{11} \frac{\partial \sigma_1}{\partial x_1} + F_{12} \left( \frac{\partial \sigma_2}{\partial x_1} + \frac{\partial \sigma_3}{\partial x_1} \right) + F_{44} \left( \frac{\partial \sigma_5}{\partial x_3} + \frac{\partial \sigma_6}{\partial x_2} \right), \quad (6-1)$$

$$E_2^f = F_{11} \frac{\partial \sigma_2}{\partial x_2} + F_{12} \left( \frac{\partial \sigma_3}{\partial x_2} + \frac{\partial \sigma_1}{\partial x_2} \right) + F_{44} \left( \frac{\partial \sigma_6}{\partial x_1} + \frac{\partial \sigma_4}{\partial x_3} \right), \quad (6-2)$$

$$E_3^f = F_{11} \frac{\partial \sigma_3}{\partial x_3} + F_{12} \left( \frac{\partial \sigma_1}{\partial x_3} + \frac{\partial \sigma_2}{\partial x_3} \right) + F_{44} \left( \frac{\partial \sigma_4}{\partial x_2} + \frac{\partial \sigma_5}{\partial x_1} \right). \quad (6-3)$$

To model the PZT thin film subject to a PFM probe, we specify the electric potential as a Lorentz function<sup>39</sup> and the stress distribution as a spherical indenter on top surface based on the Hertzian model<sup>40</sup>

$$\phi_{\text{top}}(r) = \phi_0 \frac{\gamma^2}{r^2 + \gamma^2}, \quad (7)$$

$$\sigma_{33}^{\text{tip}}(r) = -\frac{3p}{2\pi a^2} \sqrt{1 - \frac{r^2}{a^2}}, \quad (r \leq a), \quad (8)$$

in which  $\phi_0$  is the tip bias,  $r$  is the distance from the tip,  $\gamma$  is the half width at half-maximum of applied bias,  $p$  is the mechanical load, and  $a$  is the radius of the contact area.

In our simulation, we established a model with  $\text{Pb}(\text{Zr}_{0.2}\text{Ti}_{0.8})\text{O}_3$  thin film epitaxially grown on  $\text{SrTiO}_3$  (STO) substrate. A semi-implicit spectral method<sup>41</sup> was employed to solve the LGD equation with periodical boundary conditions applied along  $x$  and  $y$  directions. The top surface of the film is assumed to be stress free in the absence of tip load. Under the PFM probe indenter,  $\sigma_{33}$  on the top surface is defined from Eq. (8). The film is constrained by  $-1.5\%$  in-plane compressive strain. The simulation size is discretized into a realistic 3D mesh of  $128\Delta x \times 128\Delta x \times 32\Delta x$ , in which  $\Delta x$  is set as 1.0 nm. The thicknesses of the film and the substrate are assumed to be  $25\Delta x$  and  $5\Delta x$ , respectively. The half-width of the PFM probe and the tip contact radius are set to be  $\gamma = 10$  nm and  $a = 5$  nm, respectively. The gradient energy coefficients are set to be  $G_{11}/G_{110} = 0.6$  while  $G_{110} = 1.73 \times 10^{-10} \text{C}^{-2} \text{m}^4 \text{N}$ .<sup>42</sup> The FEC of lead titanate ( $\text{PbTiO}_3$ ) is reported to be in the range of  $1.0 \text{ nC/m}$ ,<sup>10</sup> while FEC of  $\text{Pb}(\text{Zr}_{0.2}\text{Ti}_{0.8})\text{O}_3$  has not been reported; therefore, we adopted  $\mu_{ij} = 1.0 \text{ nC/m}$  in our simulation. The Landau coefficients, electrostrictive coefficients, and elastic compliance constants are collected from literature.<sup>43-45</sup> The background dielectric permittivity of PZT is on the order of 5-7.<sup>46,47</sup> However, to compare the experimental results with the real samples, we used background dielectric permittivity of 50, as suggested from literature.<sup>48</sup>

We started with a 25 nm thick  $\text{Pb}(\text{Zr}_{0.2}\text{Ti}_{0.8})\text{O}_3$  consisting of a single tetragonal domain (along  $+z$ ,  $P = P_s = +0.7 \text{ C/m}^2$ ), which resembles the fully upward polarized PZT. The in-plane compressive strain from the substrate ensured that only  $180^\circ$  switching is allowed. The force exerted by the PFM tip at the center of top surface was assumed to be 300 nN. The applied tip bias was swept between  $-4$  and  $4$  V while the bottom electrode was grounded. We first considered the effect of longitudinal flexocoupling coefficients (FCC) by choosing  $F_{11} = 5 \times 10^{-11} \text{Vm}^2\text{N}^{-1}$  and  $F_{12} = F_{44} = 0$ . This is because only longitudinal FCC ( $f_{11}$ ) of  $\text{PbTiO}_3$  was reported.<sup>12</sup>

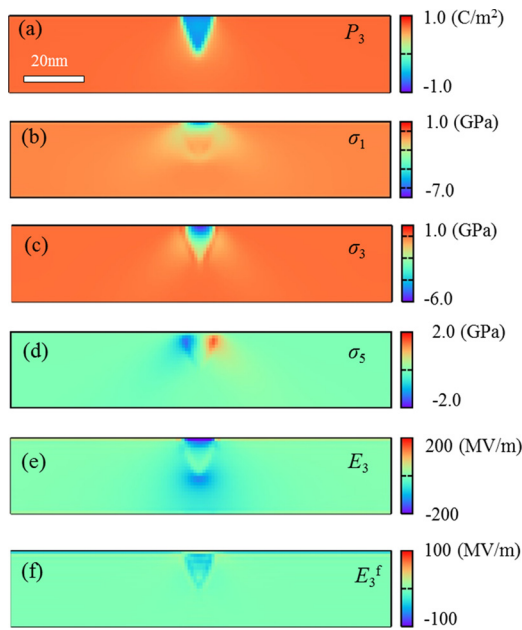


FIG. 1. 2D plot ( $x$ - $z$  plane) of (a) ferroelectric polarization component ( $P_z$ ), (b)–(d) stress distribution ( $\sigma_1$ ,  $\sigma_3$ , and  $\sigma_5$ ), (e) electric field component ( $E_3$ ), and (f) flexoelectric field component ( $E_3^f$ ) in (001) oriented single domain  $\text{Pb}(\text{Zr}_{0.2}\text{Ti}_{0.8})\text{O}_3$  thin film subject to 300 nN mechanical load and 1.5 V bias from a PFM probe.

( $F_{11}$  is recalculated from  $f_{11}$ .) The effect of  $F_{12}$  and  $F_{44}$  on switching will be discussed later. Fig. 1 shows a 2D ( $x$ - $z$  plane) snapshot of the domain structure, stress ( $\sigma_1$ ,  $\sigma_3$ , and  $\sigma_5$ ), and field distribution when the bias increases to 1.5 V. A downward nucleated nanodomain (Fig. 1(a)) and local compressive stresses (both in-plane and out-of-plane, Figs. 1(b)–1(d)) are clearly seen beneath the probe. The maximum electric field ( $E_3$ ) is concentrated under the tip and at the nanodomain apex (Fig. 1(e)), acting as the driving force of domain switching. Based on Eq. (6-3), the flexoelectric field ( $E_3^f$ ) is purely induced by stress gradient ( $d\sigma_3/dx_3$ ) when  $F_{12} = F_{44} = 0$ . Due to the large compressive stress under the tip,  $E_3^f$  is always negative (along  $-x_3$ ) during switching although  $E_3$  is bi-polar. The flexoelectric field reaches 100 MV/m near surface (Fig. 1(f)), which is in agreement with literature.<sup>20</sup>  $E_3^f$  is comparable with  $E_3$  and close to the coercive field of PZT, implying that the flexoelectric field could strongly affect the ferroelectric switching at nanoscale.

To separate the effect of electric bias, tip pressure, and flexoelectricity and to identify each of their roles in the switching process, we compared three typical scenarios: (a) pure electric switching from tip with no mechanical load, (b) electric switching under 300 nN probe load without flexoelectric effect (by artificially setting  $F_{11} = 0$ ), and (c) electric switching under 300 nN probe load and flexoelectric effect. The tip bias was swept from 0 V  $\sim$  4 V  $\sim$  0 V  $\sim$  -4 V  $\sim$  0 V. Fig. 2 illustrates the domain structures for (a)–(c) under three typical tip biases (2 V, 0 V, and -2 V) during switching. In all three cases, the downward/upward nanodomain nucleated beneath the PFM tip, continued to grow in a cone-like morphology, reached the bottom surface (so-called ferroelectric domain breakdown), and eventually widened into a cylindrical domain. The switching processes are symmetric for both (a) and (b). However, the compressive stress from 300 nN tip load suppressed the dipole moment and the spontaneous polarization, resulting in a reduced nucleated domain size (b<sub>1</sub>, b<sub>3</sub>) and slower switching process compared to scenario (a<sub>1</sub>, a<sub>3</sub>). On the contrary, it is clearly seen that the flexoelectric effect remarkably accelerated the forward switching (c<sub>1</sub>) and inhibited the reverse switching (c<sub>3</sub>), due to the unidirectional flexoelectric field, which either superimposes or counteracts the applied electric field. Our phase-field simulations on the ferroelectric switching behavior agree with thermodynamic analysis on the total free energy profile modified by different energy contributions.<sup>20,22</sup> The symmetric double well energy profile in the absence of external stress and electric field is asymmetrically changed by the flexoelectric field induced by the inhomogeneous strain, and thus favoring the unidirectional switching (Fig. 2(c)). On the other hand, the homogeneous strain modifies the free energy profile symmetrically, so that the forward and backward switchings are equivalent.

We thus performed a series of simulations with different PFM tip loads from  $p = 100$  to 500 nN, with flexoelectric effect on and off. The polarization-voltage (P-V) hysteresis loops are compared in Figs. 3(a) and 3(b), and the dependence of coercive biases and remanent polarizations ( $P_r$ ) on tip pressures are shown in Figs. 3(c) and 3(d). The polarization is calculated as an average of a  $10 \times 10 \times 10 \text{ nm}^3$  local volume beneath the tip which approximates the effective region from which the PFM response is obtained. From Fig. 3(a), the P-V loops transform from a classic square shape of hard PZT to much narrower shape mostly seen in soft PZT

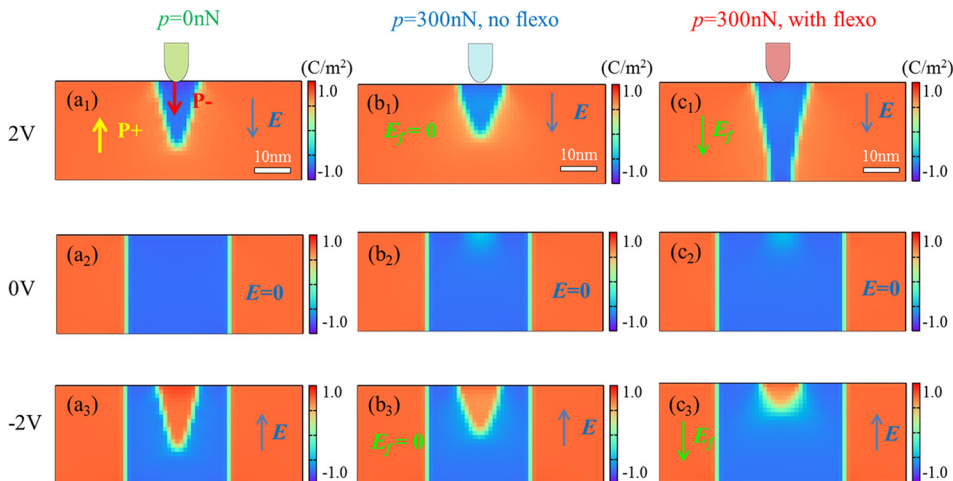


FIG. 2. (a) Comparison of ferroelectric switching behaviors in three typical scenarios: (a) pure electric switching from tip with no mechanical load, (b) electric switching under 300 nN probe load but no flexoelectric effect, and (c) electric switching with 300 nN probe load and flexoelectric effect.

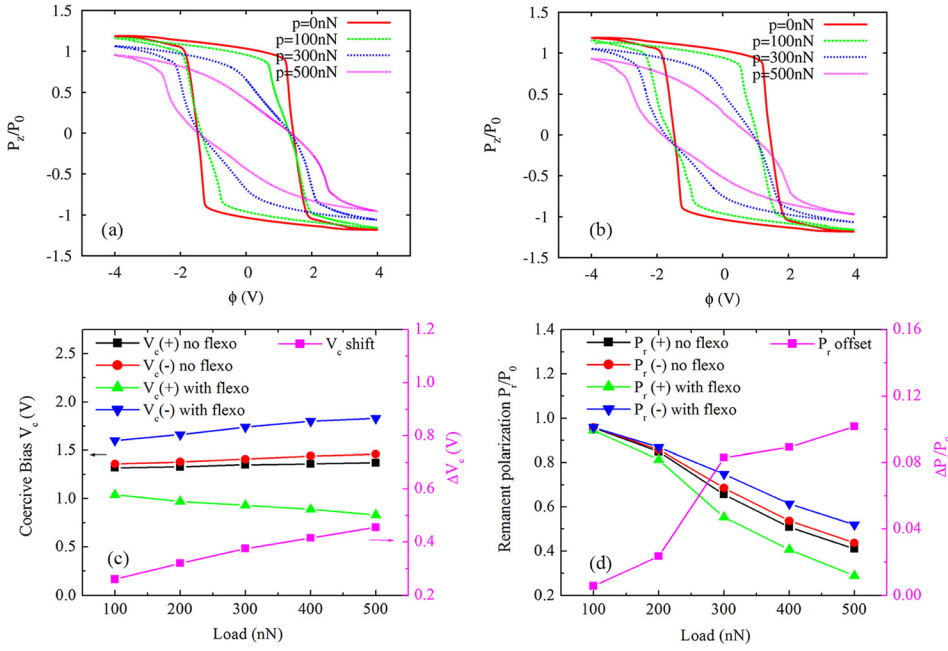


FIG. 3. Polarization-voltage (P-V) hysteresis loops under different tip pressures (a) without flexoelectric effect and (b) with flexoelectric effect. ( $P_0 = 0.7 \text{ C/m}^2$ ,  $P_z$  is calculated as an average in a  $10 \times 10 \times 10 \text{ nm}^3$  region beneath the tip.) (c) Dependence of forward/reverse coercive bias ( $V_c(+)/V_c(-)$ ) and bias shift ( $\Delta V_c$ ) on the mechanical load pressure ( $p$ ). (d) Dependence of remanent polarizations ( $P_r$ ) and their offset ( $\Delta P_r$ ) on the mechanical load pressure in reduced unit.

when the tip load increases. The remanent polarization significantly reduces by  $\sim 50\%$  from  $p = 0$  to  $p = 500 \text{ nN}$ , and the coercive bias slightly increases with increasing tip pressures, indicating that the switching becomes more difficult under large compressive strain exerted by the tip load. The hysteresis loops are symmetric, i.e., the absolute values of positive and negative coercive biases ( $V_c(+)$ ,  $V_c(-)$ ) and remanent polarizations ( $P_r(+)$ ,  $P_r(-)$ ) are almost equal at the given tip load (black and red lines in (c) and (d)) because the piezoelectric effect is of inversion symmetry. On the other hand, the flexoelectric field (along  $-x_3$ ) laterally shifts the hysteresis loops along  $-V$  (Fig. 3(b)), i.e., a smaller external bias is needed for the forward switching (green line in (c)) and a larger external bias for reversing switching (blue line in (c)) compared to those without flexoelectric effect, which agrees with Fig. 2(c). This flexo-induced hysteresis loop offset also causes smaller  $P_r(+)$  (green line in (d)) and larger negative  $P_r(-)$  (blue line in (d)) at each pressure load. The flexoelectric effect is enhanced at larger tip pressure ( $p$ ), as  $V_c(+)/V_c(-)$  continues to decrease/increase with increasing  $p$  (Fig. 3(c)). Notably, the loop collapse is much larger than the loop shift (Figs. 3(a) and 3(b)), indicating that the piezoelectricity influences the switching more profoundly than the flexoelectricity at relatively small pressure loads. To decouple the piezoelectric effect on switching, we define the coercive bias shift and remanent polarization offset by

$$\Delta V_c = [|V_c^f(+)| - V_c(+)] + [|V_c^f(-)| - V_c(-)]/2, \quad (9)$$

$$\Delta P_r = [|P_r^f(+)| - P_r(+)] + [|P_r^f(-)| - P_r(-)]/2, \quad (10)$$

where those with subscripts  $f$  denote the flexoelectric effect considered. It is found that  $\Delta V_c$  reaches  $0.45 \text{ V}$ , which is more than  $30\%$  of  $V_c$  at  $p = 500 \text{ nN}$ . And  $\Delta P_r$  suddenly increases at  $p = 300 \text{ nN}$ , a pressure value at which flexoelectric effect is possibly enhanced. Both  $\Delta V_c$  and  $\Delta P_r$  increase with tip load (pink lines in Figs. 3(c) and 3(d)) as flexoelectric field increases with PFM tip pressure.

It should be noted that there exist large discrepancies in FECs of perovskite oxides between experimental

measurement ( $\sim 10^1 - 10^2 \mu\text{C/m}$ )<sup>49–52</sup> and theoretical calculation ( $\sim 10^0 - 10^1 \text{ nC/m}$ ).<sup>10,53</sup> This difference could arise since FECs are measured at a high temperature in experiment and at  $0 \text{ K}$  in DFT calculation. Experimentally measured large flexoelectric coefficients can have other contributions, such as breaking of macroscopic centric symmetry in paraelectric phases.<sup>54</sup> This difference becomes much smaller for FCCs (in the range of  $10^1 - 10^2 \text{ V}$ ) since FECs scale with susceptibility  $\chi$ , which is much larger in experimental measurement than in the DFT calculation.<sup>12</sup> Therefore, the less temperature dependent FCCs can be considered fundamental properties of material. Furthermore, the calculated FCC values for different perovskites are mostly within one order of magnitude (e.g.:  $f_{11} \sim [10 \text{ V}, 20 \text{ V}]$  for  $\text{BaTiO}_3$ ,  $\text{PbTiO}_3$ , and  $\text{SrTiO}_3$ <sup>11</sup> and  $f_{11} = 5 \text{ V}$  for  $\text{Ba}_{0.5}\text{Sr}_{0.5}\text{TiO}_3$ <sup>53</sup>). Therefore, in this work, we choose flexocoupling coefficient  $f_{ij} \sim 10 \text{ V}$  ( $F_{ij} \sim 10^{-11} \text{ Vm}^2\text{N}^{-1}$ ) based on DFT calculations. We further studied the dependence of critical bias of ferroelectric domain breakdown (FDB) on FCCs under  $300 \text{ nN}$  tip pressure, as shown in Fig. 4. Since the domain nucleation and switching are mainly driven by the out-of-plane field

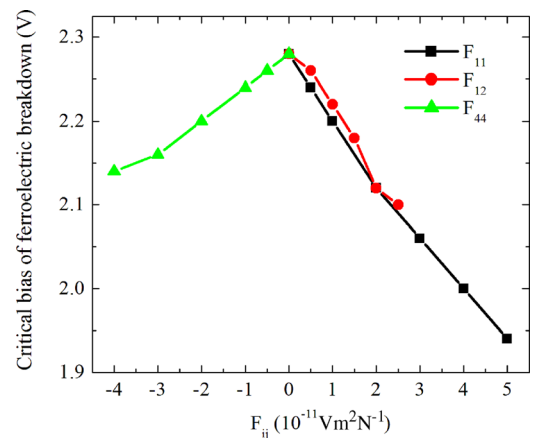


FIG. 4. Dependence of critical bias of ferroelectric domain breakdown on the longitudinal ( $F_{11}$ ), transverse ( $F_{12}$ ), and shear ( $F_{44}$ ) flexocoupling coefficients. (When varying one flexocoupling coefficient, the other two are kept to be zero.)

component ( $E_3$  and  $E_3^f$ ), and the stress gradient  $\partial\sigma_1/\partial x_3$  and  $\partial\sigma_3/\partial x_3$  are negative from stress distribution (Figs. 1(b)–1(d)), based on Eq. (6-3), positive  $F_{11}$  and  $F_{12}$  result in downward (negative) flexoelectric fields that reduce the critical bias of FDB. On the other hand,  $\partial\sigma_5/\partial x_1$  is positive, so that negative  $F_{44}$  would reduce the FDB critical bias. The FDB critical bias decreases  $\sim 20\%$  at  $F_{11} = 5 \times 10^{-11} \text{Vm}^2\text{N}^{-1}$ , and  $\sim 7\%$  at  $F_{44} = -4 \times 10^{-11} \text{Vm}^2\text{N}^{-1}$  compared to that of no flexoelectric effect. This difference is attributed to the larger stress gradient of  $\partial\sigma_3/\partial x_3$  compared to  $\partial\sigma_5/\partial x_1$ . Our results indicate that the longitudinal FCC ( $F_{11}$ ) and transverse FCC ( $F_{12}$ ) predominantly influence the FDB than the shear FCC ( $F_{44}$ ) in tip-surface ferroelectric nanojunctions.

In summary, we have implemented phase-field modeling to isolate the otherwise coupled piezoelectric and flexoelectric effects on the bipolar electro-mechanical switching in  $\text{Pb}(\text{Zr}_{0.2}\text{Ti}_{0.8})\text{O}_3$  thin film. It is revealed that the PFM probe induced mechanical strain symmetrically modifies the remnant polarization, coercive field, and shape of the hysteresis loops, and thus, no specific switching polarity is favored. On the other hand, the unipolar flexoelectricity due to the strain gradient from the tip pressure favors unidirectional switching and results in lateral offset of the P–V hysteresis loop. This flexoelectric effect is further enhanced at a large tip pressure. Finally, the longitudinal and transverse flexocoupling coefficients are found to influence the domain switching and ferroelectric breakdown more significantly than shear coefficients in the tip-surface ferroelectric nanojunctions.

This research was sponsored by the Division of Materials Sciences and Engineering, Office of Science, Basic Energy Sciences, U.S. Department of Energy. A portion of this research was conducted at the Center for Nanophase Materials Sciences, which is a DOE Office of Science User Facility. The phase-field simulation was collaborated with Professor Long-Qing Chen at Penn State, which is supported by the U.S. Department of Energy, Office of Basic Energy Sciences, Division of Materials Sciences and Engineering under Award No. DE-FG02-07ER46417. The author would thank Dr. Yijia Gu for the useful discussion and comments.

<sup>1</sup>O. Auciello, J. F. Scott, and R. Ramesh, *Phys. Today* **51**(7), 22–27 (1998).

<sup>2</sup>A. Gruverman and A. Kholkin, *Rep. Prog. Phys.* **69**(8), 2443–2474 (2006).

<sup>3</sup>J. F. Scott, *Science* **315**(5814), 954–959 (2007).

<sup>4</sup>S. M. Kogan, “Piezoelectric effect during inhomogeneous deformation and acoustic scattering of carriers in crystals,” *Sov. Phys.-Solid State* **5**(10), 2069–2070 (1964).

<sup>5</sup>P. Zubko, G. Catalan, and A. K. Tagantsev, *Annu. Rev. Mater. Res.* **43**, 387–421 (2013).

<sup>6</sup>P. V. Yudin and A. K. Tagantsev, *Nanotechnology* **24**(43), 432001 (2013).

<sup>7</sup>H. Le Quang and Q. C. He, *Proc. R. Soc. A* **467**(2132), 2369–2386 (2011).

<sup>8</sup>L. L. Shu, X. Y. Wei, T. Pang, X. Yao, and C. L. Wang, *J. Appl. Phys.* **110**, 104106 (2011).

<sup>9</sup>L. L. Shu, X. Y. Wei, T. Pang, X. Yao, and C. L. Wang, *J. Appl. Phys.* **116**, 129901 (2014).

<sup>10</sup>R. Maranganti and P. Sharma, *Phys. Rev. B* **80**, 054109 (2009).

<sup>11</sup>J. W. Hong, G. Catalan, J. F. Scott, and E. Artacho, *J. Phys.: Condens. Matter* **22**, 112201 (2010).

<sup>12</sup>J. W. Hong and D. Vanderbilt, *Phys. Rev. B* **88**, 174107 (2013).

<sup>13</sup>P. V. Yudin, A. K. Tagantsev, E. A. Eliseev, A. N. Morozovska, and N. Setter, *Phys. Rev. B* **86**, 134102 (2012).

<sup>14</sup>A. N. Morozovska, E. A. Eliseev, M. D. Glinchuk, L. Q. Chen, and V. Gopalan, *Phys. Rev. B* **85**, 094107 (2012).

<sup>15</sup>E. A. Eliseev, P. V. Yudin, S. V. Kalinin, N. Setter, A. K. Tagantsev, and A. N. Morozovska, *Phys. Rev. B* **87**, 054111 (2013).

<sup>16</sup>Y. J. Gu, M. L. Li, A. N. Morozovska, Y. Wang, E. A. Eliseev, V. Gopalan, and L. Q. Chen, *Phys. Rev. B* **89**, 174111 (2014).

<sup>17</sup>R. Ahluwalia, A. K. Tagantsev, P. Yudin, N. Setter, N. Ng, and D. J. Srolovitz, *Phys. Rev. B* **89**, 174105 (2014).

<sup>18</sup>H. T. Chen, A. K. Soh, and Y. Ni, *Acta Mech.* **225**(4–5), 1323–1333 (2014).

<sup>19</sup>G. Catalan, A. Lubk, A. H. G. Vlooswijk, E. Snoeck, C. Magen, A. Janssens, G. Rispens, G. Rijnders, D. H. A. Blank, and B. Noheda, *Nat. Mater.* **10**(12), 963–967 (2011).

<sup>20</sup>H. Lu, C. W. Bark, D. E. de los Ojos, J. Alcalá, C. B. Eom, G. Catalan, and A. Gruverman, *Science* **336**(6077), 59–61 (2012).

<sup>21</sup>J. Ocenasek, H. Lu, C. W. Bark, C. B. Eom, J. Alcalá, G. Catalan, and A. Gruverman, *Phys. Rev. B* **92**, 035417 (2015).

<sup>22</sup>Y. J. Gu, Z. J. Hong, J. Britson, and L. Q. Chen, *Appl. Phys. Lett.* **106**, 022904 (2015).

<sup>23</sup>L. M. Jiang, Y. C. Zhou, Y. Zhang, Q. Yang, Y. J. Gu, and L. Q. Chen, *Acta Mater.* **90**, 344–354 (2015).

<sup>24</sup>A. Gruverman, B. J. Rodriguez, A. I. Kingon, R. J. Nemanich, A. K. Tagantsev, J. S. Cross, and M. Tsukada, *Appl. Phys. Lett.* **83**(4), 728–730 (2003).

<sup>25</sup>E. J. Guo, R. Roth, S. Das, and K. Dorr, *Appl. Phys. Lett.* **105**, 012903 (2014).

<sup>26</sup>N. Balke, I. Bdkin, S. V. Kalinin, and A. L. Kholkin, *J. Am. Ceram. Soc.* **92**(8), 1629–1647 (2009).

<sup>27</sup>M. Alexe, A. Gruverman, C. Harnagea, N. D. Zakharov, A. Pignolet, D. Hesse, and J. F. Scott, *Appl. Phys. Lett.* **75**(8), 1158–1160 (1999).

<sup>28</sup>A. Gruverman, O. Auciello, and H. Tokumoto, *Annu. Rev. Mater. Sci.* **28**, 101–123 (1998).

<sup>29</sup>A. Gruverman, O. Auciello, R. Ramesh, and H. Tokumoto, *Nanotechnology* **8**, A38–A43 (1997).

<sup>30</sup>D. A. Bonnell, S. V. Kalinin, A. L. Kholkin, and A. Gruverman, *MRS Bull.* **34**(9), 648–657 (2009).

<sup>31</sup>H. L. Hu and L. Q. Chen, *Mater. Sci. Eng. A* **238**(1), 182–191 (1997).

<sup>32</sup>S. V. Kalinin, B. J. Rodriguez, S. Jesse, Y. H. Chu, T. Zhao, R. Ramesh, S. Choudhury, L. Q. Chen, E. A. Eliseev, and A. N. Morozovska, *Proc. Natl. Acad. Sci. U. S. A.* **104**(51), 20204–20209 (2007).

<sup>33</sup>P. Maksymovych, S. Jesse, M. Huijben, R. Ramesh, A. Morozovska, S. Choudhury, L. Q. Chen, A. P. Baddorf, and S. V. Kalinin, *Phys. Rev. Lett.* **102**, 017601 (2009).

<sup>34</sup>B. J. Rodriguez, S. Choudhury, Y. H. Chu, A. Bhattacharyya, S. Jesse, K. Seal, A. P. Baddorf, R. Ramesh, L. Q. Chen, and S. V. Kalinin, *Adv. Funct. Mater.* **19**(13), 2053–2063 (2009).

<sup>35</sup>Y. Cao, A. V. Ievlev, A. N. Morozovska, L. Q. Chen, S. V. Kalinin, and P. Maksymovych, *Appl. Phys. Lett.* **107**, 022903 (2015).

<sup>36</sup>L. Q. Chen, *J. Am. Ceram. Soc.* **91**(6), 1835–1844 (2008).

<sup>37</sup>Y. L. Li, S. Y. Hu, Z. K. Liu, and L. Q. Chen, *Acta Mater.* **50**(2), 395–411 (2002).

<sup>38</sup>Y. J. Gu, Ph.D. dissertation, The Pennsylvania State University, 2014.

<sup>39</sup>S. Choudhury, J. X. Zhang, Y. L. Li, L. Q. Chen, Q. X. Jia, and S. V. Kalinin, *Appl. Phys. Lett.* **93**, 162901 (2008).

<sup>40</sup>A. C. Fischer-Cripps, *Introduction to Contact Mechanics*, 2nd ed. (Springer, New York, 2007).

<sup>41</sup>L. Q. Chen and J. Shen, *Comput. Phys. Commun.* **108**(2–3), 147–158 (1998).

<sup>42</sup>F. Xue, J. J. Wang, G. Sheng, E. Huang, Y. Cao, H. H. Huang, P. Munroe, R. Mahjoub, Y. L. Li, V. Nagarajan, and L. Q. Chen, *Acta Mater.* **61**(8), 2909–2918 (2013).

<sup>43</sup>M. J. Haun, Z. Q. Zhuang, E. Furman, S. J. Jang, and L. E. Cross, *Ferroelectrics* **99**, 45–54 (1989).

<sup>44</sup>M. J. Haun, E. Furman, S. J. Jang, H. A. McKinstry, and L. E. Cross, *J. Appl. Phys.* **62**(8), 3331–3338 (1987).

<sup>45</sup>M. J. Haun, E. Furman, S. J. Jang, and L. E. Cross, *Ferroelectrics* **99**, 13–25 (1989).

<sup>46</sup>A. K. Tagantsev, G. Gerra, and N. Setter, *Phys. Rev. B* **77**(17), 174111 (2008).

<sup>47</sup>A. N. Morozovska, E. A. Eliseev, S. V. Svechnikov, A. D. Krutov, V. Y. Shur, A. Y. Borisevich, P. Maksymovych, and S. V. Kalinin, *Phys. Rev. B* **81**(20), 205308 (2010).

<sup>48</sup>G. Rupperecht and R. O. Bell, *Phys. Rev.* **135**(3A), A748 (1964).

<sup>49</sup>W. H. Ma and L. E. Cross, *Appl. Phys. Lett.* **81**(18), 3440–3442 (2002).

<sup>50</sup>W. H. Ma and L. E. Cross, *Appl. Phys. Lett.* **82**(19), 3293–3295 (2003).

<sup>51</sup>W. H. Ma and L. E. Cross, *Appl. Phys. Lett.* **86**(7), 072905 (2005).

<sup>52</sup>W. H. Ma and L. E. Cross, *Appl. Phys. Lett.* **88**(23), 232902 (2006).

<sup>53</sup>I. Ponomareva, A. K. Tagantsev, and L. Bellaiche, *Phys. Rev. B* **85**(10), 104101 (2012).

<sup>54</sup>A. Biancoli, C. M. Fancher, J. L. Jones, and D. Damjanovic, *Nat. Mater.* **14**(2), 224–229 (2015).